THE JOURNAL OF PHYSICAL CHEMISTRY A

Article

Effect of Spectral Density Shapes on the Excitonic Structure and Dynamics of the Fenna-Matthews-Olson Trimer From Chlorobaculum Tepidum

Adam Kell, Robert E. Blankenship, and Ryszard J Jankowiak

J. Phys. Chem. A, **Just Accepted Manuscript** • DOI: 10.1021/acs.jpca.6b03107 • Publication Date (Web): 20 Jul 2016

Effect of Spectral Density Shapes on the Excitonic Structure and Dynamics of the Fenna-Matthews-Olson Trimer from *Chlorobaculum tepidum*

Adam Kell,[1] Robert E. Blankenship,[2] and Ryszard Jankowiak[1,3,*]

[1]Department of Chemistry and [3]Department of Physics, Kansas State University, Manhattan, KS 66506, USA

[2]Departments of Chemistry and Biology, Washington University in St. Louis, St. Louis, MO 63130, USA

ABSTRACT: The Fenna-Matthews-Olson (FMO) trimer (composed of identical subunits) from the green sulfur bacterium *Chlorobaculum tepidum* is an important protein model system to study exciton dynamics and excitation energy transfer (EET) in photosynthetic complexes. In addition, FMO is a popular model for excitonic calculations, with many theoretical parameter sets reported describing different linear and nonlinear optical spectra. Due to fast exciton relaxation within each subunit, intermonomer EET results predominantly from the lowest energy exciton states (contributed to by BChl *a* 3 and 4). Using experimentally determined shapes for the spectral densities, simulated optical spectra are obtained for the entire FMO trimer. Simultaneous fits of low-temperature absorption, fluorescence and hole-burned spectra place constraints on the determined pigment site energies; providing a new Hamiltonian that should be further tested to improve modeling of 2D electronic spectroscopy data and our understanding of coherent and dissipation effects in this important protein complex.

Introduction

The Fenna-Matthews-Olson protein complex (FMO) is found mainly in green sulfur bacteria (GSB) and facilitates excitation energy transfer (EET) from light-harvesting chlorosomes to the reaction center.[1,2] It was the first pigment-protein complex to have the crystal structure determined[3] and X-ray crystallography data for FMO from several GSB are available,[4–6] which reveal very similar features for FMO of *Chlorobaculum* (*C.*) *tepidum*, *Prosthecochloris* (*Pr.*) *aestuarii* and *Pelodictyon phaeum*. That is, FMO is a homotrimer with each monomer binding seven to eight bacteriochlorophyll (BChl) *a* pigments enclosed in a series of β sheets. The existence of BChl *a* 8 was discovered more recently[7] and its occupancy in isolated complexes is known to vary.[4,5,8]

The wealth of crystallography data on FMO is particularly appealing for structure-based calculations. Recent studies have been undertaken to calculate pigment site energies based solely on chlorophyll conformations using quantum chemical and optimization approaches.[9,10] While such atomistic studies represent important advances in structure-based modeling, the reported energies (and ordering) for FMO[9] cannot explain experimental data as of yet. However, such studies reveal that site energies critically depend on the protein binding pocket and pigment conformations. Therefore, at this point the best approach for elucidating site energies is simultaneous calculations of optical spectra using an optimization algorithm (vide infra).

Much of the interest in FMO is due to the results of pump-probe and 2D electronic spectroscopy (2DES) measurements, where quantum beats were observed in the 19 K polarized pump-probe signal[11] and 2D maps at 77 K[12] and room temperature.[13] The relaxation of localized and delocalized states can be treated by Förster[14,15] and Redfield[16–18] theories, respectively. Since photosynthetic complexes often fall within an intermediate regime between the two limits of weak and strong coupling, various other theoretical methods have been proposed, often with FMO as a model system. For example, Redfield,[19–21] modified Redfield,[22] correlated driving-dissipation equation,[23] zeroth order functional expansion master equation,[24,25] equation-of-motion phase-matching,[26] hierarchical equations-of-motion,[27–30] and numerical path integral[31,32] approaches have been applied in the interpretation of population dynamics and coherent oscillations involved in EET within FMO.

While fast timescale kinetics (on the order of femtoseconds) can be described with only intramonomer exciton relaxation, intermonomer EET is important when considering steady-state and frequency-domain spectra, e.g., fluorescence and hole-burned (HB) spectra.[33] In order to generate the most physically realistic Hamiltonian possible, as many constraints need to be placed on the fitting process as possible. That is, the entire trimer has to be taken into account in order to properly describe various optical spectra simultaneously.[33,34] For example, linear absorption spectra have been shown to differ for various FMO complexes reported in the literature,[35] suggesting that site energies generated from simulations of only absorption spectra can vary for different samples or laboratories.

In this work, Redfield theory is applied in order to generate an optimized Hamiltonian for the FMO trimer from *C. tepidum*. Since the intermonomer dipole coupling is weak, Generalized Förster theory[36,37] is used to describe three excitonic domains (corresponding to the pigments bound by each protein subunit). That is, exciton delocalization is restricted to a single domain and interdomain EET between lowest energy excitons of each domain is described by the Förster rate equation.[14,15] However, BChl *a* 8 is included in the domain of the neighboring protein monomer, as this pigment has a larger intermonomer coupling constant with BChl *a* 1 of the adjacent subunit than any intramonomer couplings.

Theory

Simulated spectra are calculated following Generalized Förster theory,[36,37] with exciton lineshapes and relaxation within excitonic domains described by a non-Markovian density matrix approach.[18] Exciton delocalization is restricted to three distinct domains with each domain corresponding to the pigments bound by a protein subunit (with the exception for BChl *a* 8 mentioned above). BChl *a* atomic coordinates are taken from the X-ray structure (PDB ID: 3ENI)[4] and Model A neglected BChl *a* 8 while Models B and C included full occupancy of BChl *a* 8.[8] Electronic coupling constants (V) are calculated using the TrEsp method[38] with an effective transition dipole strength $|\mu|^2 = 25.2$ D^2 (which includes contributions of the relative dielectric of the medium).[33] This value was chosen in order to yield coupling constants similar to those in column 4 in Table 1 of ref 19. In addition, BChl *a* ground state vibrational modes determined from the ΔFLN spectrum[40] were included ($S_{vib} = 0.4$) by convolution of Lorentzian peaks with the excitonic lineshape.

Three models are considered in the following sections, with the spectral density (weighted one-phonon profile) assumed to be a lognormal distribution.[39] In Model A, the spectral density shape is site-independent and is determined from difference fluorescence line narrowing (ΔFLN) data,[40] with $\omega_c = 38$ cm^{-1}, $\sigma = 0.7$,[39] and $S = 0.3$, where ω_c, σ and S correspond to the cutoff frequency, standard deviation, and Huang-Rhys factor, respectively. S is defined as the area of the spectral density at zero temperature, that is,

$$S = \int_0^\infty J(\omega)\, d\omega \qquad (1)$$

Inhomogeneous broadening is site-dependent for Model A. In Model B, inhomogeneous broadening is site-independent while $S = 0.3$ and 2.2 for BChl *a* 3 and all other BChl *a*, respectively.

Finally for Model C, BChl *a* 3 has the same spectral density shape (with $S = 0.4$) as the previous models, but for higher energy pigments, a broader spectral density shape is used, i.e., $\omega_c = 45$ cm^{-1}, $\sigma = 0.85$ and $S = 0.4$. These parameters are determined from excitation-dependent FLN calculations of the B777 complex[41] (BChl *a* bound to a single α helix protein), while S is assumed to be site-independent.

The fwhm of inhomogeneous broadening for BChl *a* 3 (75 cm^{-1}) is constrained by the width of the 825 nm absorption and fluorescence (0,0) bands. All other BChl *a* have fwhm of 125 cm^{-1}, in order to better fit the high-energy absorption features. Pigment site energies are adjusted to provide simultaneous fits to absorption, fluorescence and persistent nonresonant HB spectra. In order to optimize the fits to experimental data, a Nelder-Mead simplex[42] algorithm was utilized to search the solution space and minimize the root-mean-square deviation

$$RMSD = \sqrt{\frac{\sum_{i=1}^{N}(y_{theo} - y_{exp})^2}{N}}, \qquad (2)$$

where N is the total number of compared points, y_{theo} and y_{exp} are the corresponding theoretical and experimental y-values, respectively.

HB spectra were best fit assuming a 60 cm^{-1} blue-shift of the post-burn site energy distributions;[33,34] suggesting that the main energy tier in the FMO protein energy landscape is about 60 cm^{-1}. The spectral contributions of BChl *a* pigments to the absorption spectrum can be calculated according to

$$a_m(\omega) = \omega\left(\sum_M |c_{mM}|^2 |\mu_M|^2 D_M(\omega)\right)_{dis}, \qquad (3)$$

where $D_M(\omega)$ is the lineshape of exciton state M, $|c_{mM}|^2$ is the contribution number (squared eigenvector coefficient) of site m to state M, $|\mu_M|^2$ is the transition dipole strength of state M, and $\langle\ldots\rangle_{dis}$ indicates disorder averaging. The contribution numbers also define the delocalization length (inverse participation ratio) by

$$L_M = \frac{1}{\sum_m |c_{mM}|^4} \qquad (4)$$

The equations describing intradomain rates for exciton relaxation are given in ref 19. This work considers excitation by a femtosecond laser pulse and includes orientation averaging with respect to the laser polarization.

Results and Discussion

Frames A-C of Figure 1 show experimental and calculated absorption, fluorescence and persistent nonresonant (λ_B = 496.5 nm) HB spectra for Models A-C, respectively. The shape of the HB spectra was independent of laser fluence used (i.e., no shift of the lowest energy bleach was observed), indicating that this FMO sample was intact and not a mixture of intact and destabilized proteins (for details see ref 35). Frame C shows the results of simulated absorption (curves a′), fluorescence (curve b′) and nonresonant HB (curve c′) spectra using the Hamiltonian presented in Table 1 (Model C) compared to the respective experimental data (curves a-c). The lowest energy absorption (12,110 cm^{-1}) and fluorescence (12,086 cm^{-1}) bands, in addition to the lowest energy hole, are well-fit by considering the entire FMO trimer, as shown previously for a simplified model consisting of only BChl *a* 3 and 4.[33,34] In addition, only a reorganization energy (E_λ) of ~15 cm^{-1} can describe the small Stokes shift[35] and fit the narrow absorption band at 12,110 cm^{-1} (due to weaker coupling to phonon modes).

While the simulated absorption, fluorescence and nonresonant HB spectra for Model A fit the experimental curves well (frame A), the resulting population dynamics (see Figure 2) are not consistent with time-resolved spectra,[43–45] where the excitation energy is mostly located on the lowest energy exciton state within 1-10 ps. The latter indicates that the weak el-ph coupling determined experimentally for the lowest exciton state (mainly localized on BChl *a* 3) is not applicable to all higher energy states; as the slow dynamics are due to the narrow spectral density, which determines what phonon modes are available to participate in energy transfer. That is, stronger el-ph coupling is a necessary condition in order to properly describe the exciton population dynamics of FMO. The initial populations are calculated assuming excitation by a 50 fs laser pulse at 12,626 cm^{-1}.[19,22] States 6, 7 and 8 have the largest initial populations, with the lowest energy state 1 having negligible initial population. By 5 ps the population of state 1 is approximately 70% via relaxation from state 2 ($k_{21} = 1.7$ ps^{-1}). As reported previously,[19,22] state 3 decays rather slowly due to the small spatial overlap with exciton states 1 and 2.[22] The relative populations in Figure 2B are consistent with experimental data, which observed relaxation to the lowest energy state within 1–10 ps.[43–45]

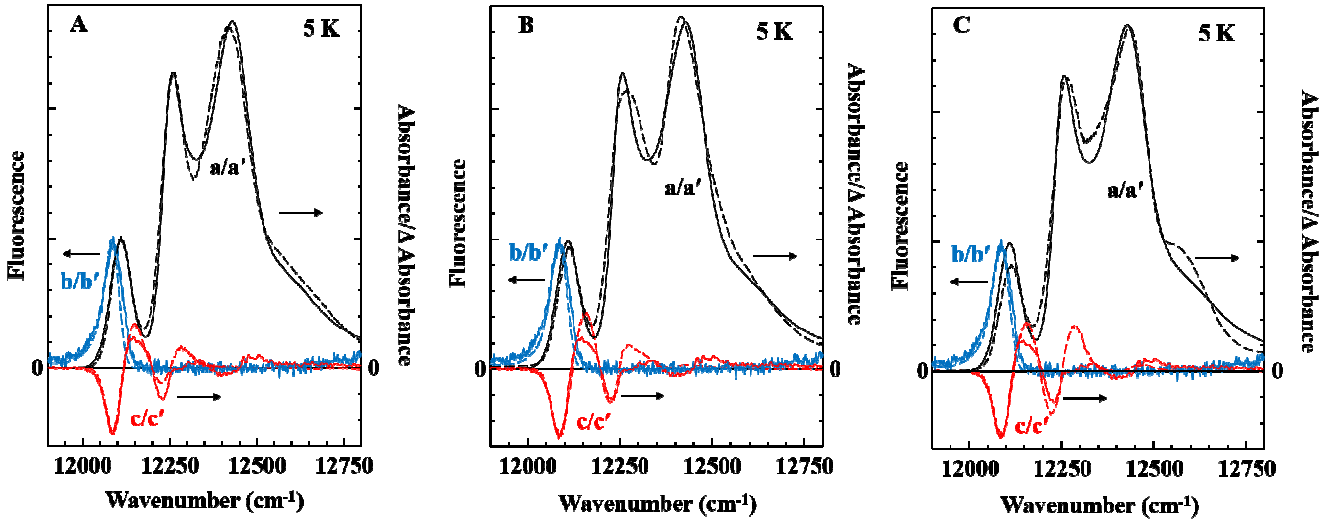

Figure 1. 5 K experimental[35] (solid) and simulated (dashed) absorption (black curves a/a′), emission (blue curves b/b′) and non-resonant HB (red curves c/c′) spectra. Frame A shows simulated spectra assuming a site-independent spectral density and site-dependent fwhms (Model A). Frame B shows fits for Model B with only one spectral density shape but two *S* factors and site-independent fwhms. Fame C shows the results for two spectral density shapes and site-dependent fwhms (Model C).

Table 1. Model C Frenkel exciton Hamiltonian for the FMO trimer in the site representation*

BChl *a*	1	2	3	4	5	6	7	8
1	12405	-87	4.2	-5.2	5.5	-14	-6.1	21
2		12505	28	6.9	1.5	8.7	4.5	4.2
3			12150	-54	-0.2	-7.6	1.2	0.6
4				12300	-62	-16	-51	-1.3
5					12470	60	1.7	3.3
6						12575	29	-7.9
7							12375	-9.3
8								12430

*All values in units of cm^{-1}

Due to the issues presented in Figure 2, the experimental data were again fit using Redfield theory and Model B. The fits are shown in frame B of Figure 1, and for simplicity all pigments have the same inhomogeneous broadening (fwhm = 75 cm^{-1}). The presence of stronger el-ph coupling increases the exciton relaxation rates as shown in frame B of Figure 2. However, the increased *S* value enhances the temperature-dependent broadening of the absorption spectrum which is inconsistent with the experimental data (see Figure 3). While the experimental spectra show only small temperature effects (even at 150 K the three bands can still be somewhat resolved), the simulated curves in frame B change more noticeably at higher temperatures. For example, the calculated spectrum at 50 K is similar to the experimental 150 K spectrum. Such a discrepancy indicates that FMO has weak el-ph coupling, consistent with literature data,[19,40,46] and only a broader spectral density shape of Model C can improve exciton dynamics and describe the absorption temperature dependence. The temperature range was chosen such that additional effects due to crossing the glass transition (150-200 K)[47,48] can be ignored.

The "type 2" absorption spectrum of *C. tepidum* (where the 12,430 cm^{-1} peak is more intense than the 12,260 cm^{-1} peak[4,49,50]) is reproduced and the intensity of the 12,260 cm^{-1} peak is found to be critically dependent on the energy values of pigments strongly coupled to BChl *a* 4 (i.e., BChls 3, 5 and 7). Oscillator strength can be redistributed between BChl *a* 4 and BChl *a* 3, 5 and 7; suggesting that BChl *a* 4 plays an important role in the FMO absorption differences between species of GSB. Note that in this work the Q_y region is well-fit with 3 BChl *a* 8 per trimer. However, this assignment could be lower as mass spectrometry results indicate both detergent- and sodium carbonate-extracted FMO complexes have on average 2-3 BChl *a* 8 per complex.[8] An occupancy of ~80%, is a more likely scenario, but determining the exact spectroscopic contribution of BChl *a* 8 is beyond the scope of this work.

Figure 4 shows triplet minus singlet (T–S), circular dichroism (CD) and linear dichroism (LD) spectra calculated using the Model C parameters from Table 1 compared to the low-temperature, experimental data.[51] The comparisons can only provide a qualitative assessment of the simulation parameters, as the absorption spectrum of ref 51 is blue-shifted compared to the absorption spectrum fitted in the main text. The implications of such shifts are described in more detail elsewhere.[35] Even so, the main features are reproduced, although some bands are shifted. For example, the low-energy bleach in the

T–S spectrum is more red-shifted for the simulated curve (a′), consistent with the above-mentioned shifts of the 825 nm absorption band. Interestingly, the low-energy fits of CD and LD are much better. In order to have a more meaningful comparison, multiple spectra (i.e., absorption, fluorescence, HB, T–S, and CD) need to be measured on a single sample in a relatively short timeframe so as to prevent destabilization of the protein. However, given uncertainties in the electron-phonon (el-ph) coupling parameters of high-energy pigments, the simulated spectra in Figure 4 fit the experimental data reasonably well.

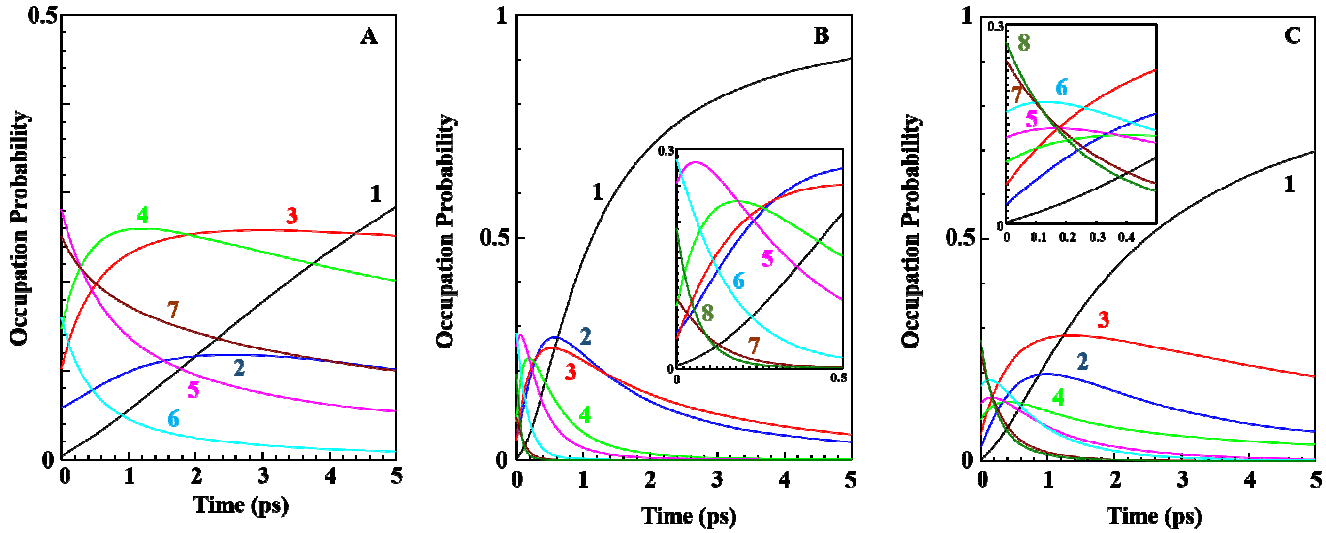

Figure 2. 5 K exciton population dynamics after initial excitation by a 50 fs laser pulse (12,626 cm^{-1}).[19,22] The initial populations are normalized to one. Frames A-C shows the results for Models A-C, respectively. The insets in frames B and C show the dynamics of the fast-decaying, high-energy states in the first 0.5 ps.

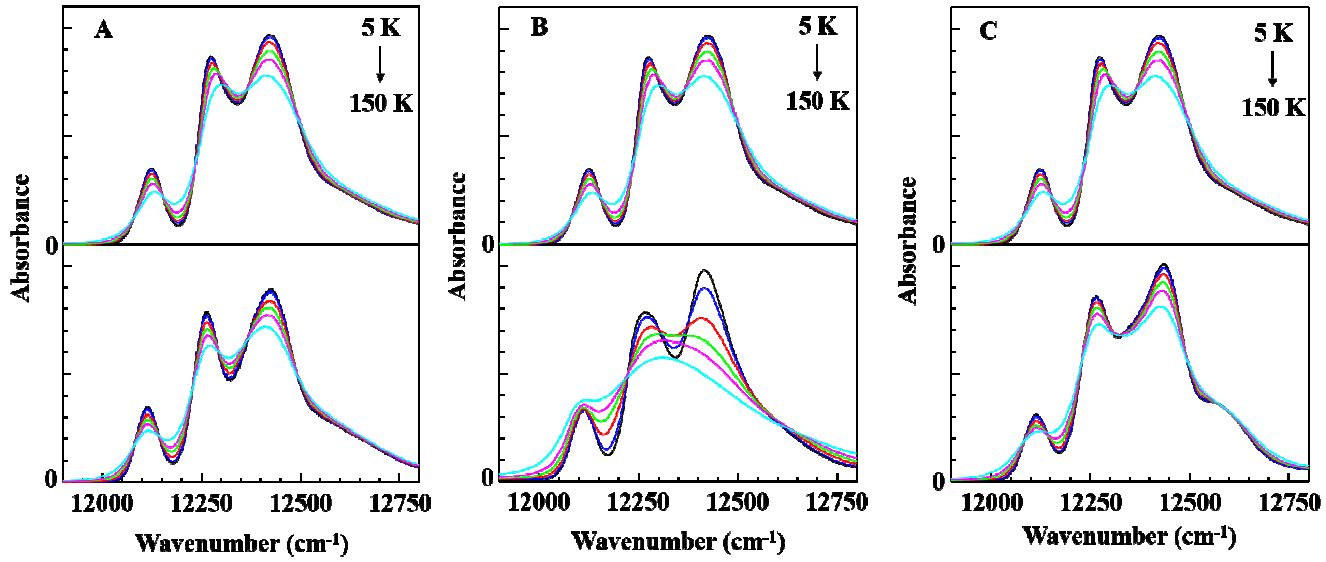

Figure 3. Experimental (top frames) and simulated (bottom frames) temperature-dependent absorption spectra measured at 5, 25, 50, 75, 100 and 150 K. Frames A-C correspond to Models A-C, respectively.

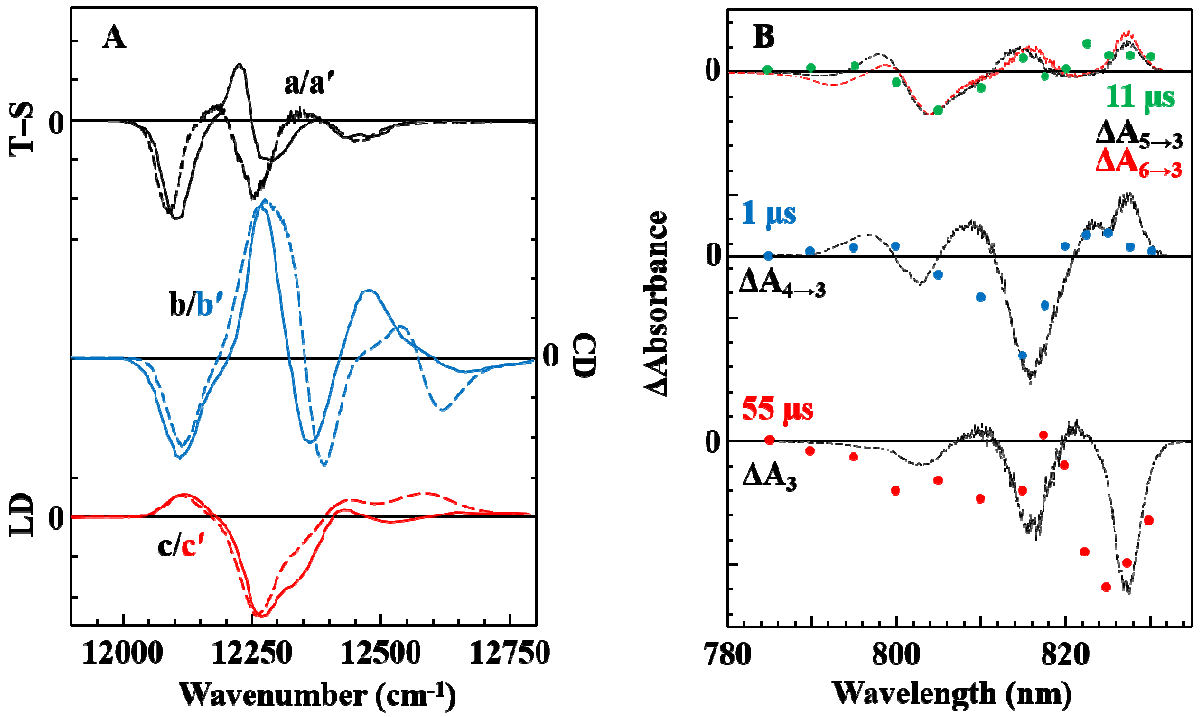

Figure 4. Frame A: 6 K experimental[51] (solid) and simulated (dashed) T–S (black curves a/a′), CD (blue curves b/b′) and LD (red curves c/c′) spectra. Frame B: Calculated ΔA spectra (dashed lines) assuming the triplet state resides on various BChl *a* compared to 20 K experimental DADS (data points).[52] ΔA_3 corresponds to the long-lived T–S spectrum, while $\Delta A_{i\rightarrow 3}$ is the bleach resulting from triplet energy transfer from BChl *a i* to BChl *a* 3. All curves are simulated using Model C parameters.

Table 2. Comparison of Model C FMO site energies and various literature Hamiltonians

BChl *a*	Model C	Ref 51	Ref 22	Ref 19	Ref 55	Ref 54
1	12 405 (4)	12 400 (3)	12 420 (4)	12 410 (3)	12 468 (6)	12 566(6)
2	12 505 (7)	12 600 (7)	12 560 (7)	12 530 (6)	12 466 (5)	12 461(3)
3	12 150 (1)	12 140 (1)	12 140 (1)	12 210 (1)	12 129 (1)	12 381(1)
4	12 300 (2)	12 280 (2)	12 315 (2)	12 320 (2)	12 410 (4)	12 494(5)
5	12 470 (6)	12 500 (5)	12 460 (5)	12 480 (5)	12 320 (2)	12 445(2)
6	12 575 (8)	12 500 (5)	12 500 (6)	12 630 (7)	12 593 (7)	12 469(4)
7	12 375 (3)	12 430 (4)	12 400 (3)	12 440 (4)	12 353 (3)	12 873(8)
8	12 430 (5)	–	–	–	–	12 598(7)

The numbers in parenthesis rank site energies from lowest (1) to highest.

In addition to the low-temperature data shown in Figure 4A, low-temperature triplet energy transfer has recently been studied for FMO.[52,53] The resulting 20 K decay associated difference spectra (DADS) are shown in Figure 4B, with calculated

ΔA spectra for the same triplet energy transfers as reported in ref 52. That is, ΔA_3 is curve a′ from Figure 4A, while $\Delta A_{i\rightarrow 3} = \Delta A_i - \Delta A_3$, where i = 4, 5 or 6 corresponds to the calculated bleach assuming BChl *a* *i* is in the triplet state. As with the T–S spectrum of ref 51, the low-energy bleach of the simulated ΔA_3 spectrum is red-shifted compared to experiment (see red dots), reflecting different spectral positions of the 825 nm absorption band. However, the $\Delta A_5 - \Delta A_3$ and $\Delta A_6 - \Delta A_3$ spectra agree with experimental results, as the absorption peak position near 805 nm (mainly contributed to by BChl *a* 5 and 6) is not as sensitive to the sample preparation as the 825 and 814 absorption peaks.[35] Overall the simulated ΔA curves using the parameters of the Model C Hamiltonian (see Table 1) agree with the conclusions of ref 52. In summary, simulated bleaching due to triplet energy transfer along the BChl *a* 5/6 → 4 → 3 pathway is consistent with experimental DADS.

Table 2 shows the site energies for the BChl *a* pigments of FMO proposed for Model C and several Hamiltonians from the literature.[19,22,51,54,55] Columns 2-6 correspond to energies found by fitting optical spectra, while the values of ref 54 in column 7 are calculated by molecular dynamics simulations. Overall the energy sets have similar trends, e.g., BChl *a* 2 has a higher site energy than BChl *a* 1. Important to notice is that only in refs 54 and 55 is BChl *a* 4 not the second lowest in energy. Figure S3 in the SI shows that such an assignment, for example ref 55, is inconsistent with HB data, which requires a smaller energy gap between BChl *a* 3 and 4 than 281 cm^{-1}.

The pigment spectral contributions for Model C are shown in Figure 5. In agreement with the current consensus,[2,53,56] BChl *a* 3 is the most red-shifted pigment and contributes ~85% to the lowest energy exciton state, while BChl *a* 4 contributes (~50%) mainly to the second exciton state at ~12,260 cm^{-1} (see Table 3). As BChl *a* 6 is located near the baseplate,[56] it has the highest site energy and is the main contributor to the highest energy exciton state; with minor contribution from BChl *a* 5. Note that a higher site energy of BChl *a* 5 is consistent with its position with respect to α helices 4 and 5.[4,57] The positive ends of the α-helix dipoles are in the vicinity of the positive difference of the electrostatic potential of BChl *a* 5 between the S_1 and S_0 states, potentially raising the pigment site energy.

It is possible that the site energy of BChl *a* 5 differs in other species of GSB; that is, as mentioned previously, the intensity of the low-temperature absorption band at 12,260 cm^{-1} was found to be sensitive to the site energy of pigments strongly coupled to BChl *a* 4. For example, as reported in Table 1 $|V_{45}|$ = 60 cm^{-1}, which is the second largest off-diagonal element in the Hamiltonian. Thus, a different energy gap between BChl *a* 4 and 5 will have significant impact on the shape of the absorption spectrum. In addition, while the local protein environment of most binding sites is highly conserved among species, there are differences near the binding site of BChl *a* 5 in *C. tepidum*[4,5] which could result in a significant change in the site energy. Note that changes in the site energy of BChl *a* 7 could have similar effects, although the binding site is very homologous between various GSB species.[4,5]

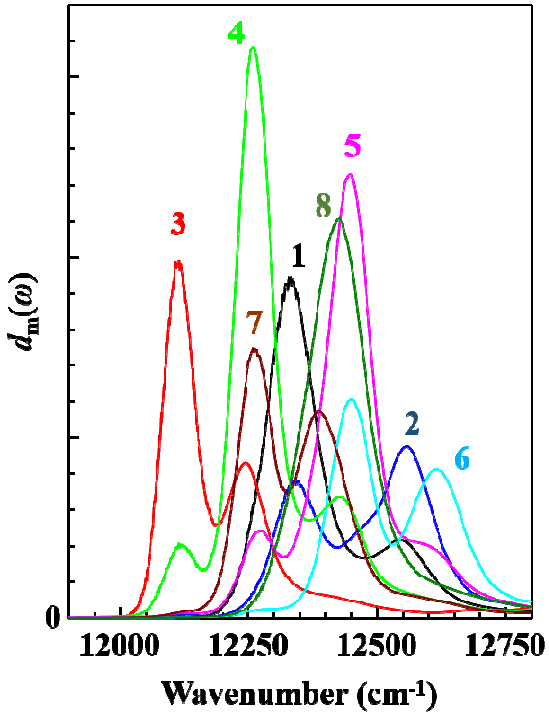

Figure 5. Model C BChl *a* contributions to absorption ($d_m(\omega)$) calculated with eq 3.

Table 3. Contribution numbers ($|c_{mM}|^2$) of sites *m* for states *M* from a simultaneous fit of spectra shown in Figure 1C.

m \ *M*	1	2	3	4	5	6	7	8
1	0.00	0.07	0.45	0.13	0.05	0.03	0.21	0.05
2	0.01	0.02	0.15	0.06	0.04	0.07	0.51	0.14
3	0.84	0.13	0.02	0.01	0.00	0.00	0.00	0.00
4	0.14	0.49	0.08	0.10	0.08	0.06	0.02	0.02
5	0.00	0.07	0.04	0.12	0.19	0.31	0.10	0.17
6	0.00	0.00	0.01	0.02	0.10	0.15	0.12	0.60
7	0.01	0.22	0.12	0.36	0.19	0.07	0.01	0.02
8	0.00	0.01	0.13	0.19	0.35	0.30	0.03	0.00
L_M	1.39	2.30	2.10	2.56	2.33	2.25	2.21	1.93

Due to its relatively recent discovery and seemingly partial occupancy, BChl *a* 8 has gained much interest into its occupancy in isolated versus in vivo FMO complexes and its role in EET. Since a small occupancy was predicted based on electron density of the X-ray structure[4] and the suggestions that BChl *a* 8 may be removed from the protein detergent[8] or polyethelyne glycol,[6] many studies neglect its presence by assuming only a negligible amount remains after protein purification. However, Wen et al.[8] showed that significant populations of BChl *a* 8 exist in various isolated FMO samples from *C. tepidum* in both detergent- and sodium carbonate-extracted samples. While theoretical studies often assign BChl *a* 8 a very blue shifted site energy (12,600-12,700 cm^{-1}),[21,54] a spectral position of ~806 nm (12,407 cm^{-1}) was proposed based on absorption changes induced by chemical oxidation at 77 and 293 K.[58] Below we report on the 5 K oxidation of FMO by

potassium ferricyanide and compare to the spectral contribution of BChl *a* 8 from Redfield calculations.

Figure 6 shows a comparison of two absorption spectra for FMO; chemically neutral (curve a) and oxidized (curve b). The oxidized sample had a concentration of ~2 M ferricyanide, which was much larger than used in the previous study.[58] The difference curve (c) indicates that a small population of the low-energy BChl *a* 3 and 4 pigments are oxidized, but the main feature is the bleach at 12,420 cm^{-1}. Bina and Blankenship[58] proposed that BChl *a* 8 should be preferentially oxidized due to its location at the interface of two protein subunits and, similar to Figure 6, observed the largest bleach ~12,400 cm^{-1}. The green curve in Figure 5 is the spectral contribution from Figure 4 for BChl *a* 8 inverted and scaled for comparison. The distribution matches the bleach at 12,420 cm^{-1} quite well and suggests that BChl *a* 8 contributes to the most intense 12,430 cm^{-1} band in *C. tepidum*. The relative absorption changes in the 12,420 cm^{-1} region indicate that curve b represents ~30% oxidation of the BChl *a* 8 population (assumed to be 3 per protein trimer). In this case, it is unlikely that BChl *a* 8 plays a role in the intensity of the 12,260 cm^{-1} absorption peak,[4] as a Q_y energy shift of –200 cm^{-1} due to the coordination state of the central magnesium ion is unlikely.[59] Based on extensive model simulations, the difference between types 1 and 2 absorption spectra for FMO of various GSB results from differing interactions of BChl *a* 4 with nearby pigments (vide supra).

Calculated Redfield rate constants for intramonomer exciton relaxation in Model C are shown in Table 4. Redfield EET occurs between two states whose energy difference matches some phonon frequency of the bath.[16,17] Thus, the rates depend on the spectral density used in calculations. Therefore, we emphasize that the spectral density shape must be experimentally established for the particular pigment-protein complex under study (e.g., in this work FMO). Only then can a reliable rate matrix be used to calculate exciton population dynamics (see Table 4). In ref 39 it was shown that the lognormal distribution for FMO (after multiplying by ω^2) can be compared to an Ohmic function with parameters from ref 22. The Ohmic parameters were determined by fitting 2D photon echo spectra (with E_λ = 35 cm^{-1}), but should not be used in calculations as the Ohmic function cannot properly describe the phonon sideband. However, the lognormal spectral density used in this work for high-energy pigments (E_λ ~ 25 cm^{-1}) is capable of describing both the absorption lineshape and exciton population dynamics; although E_λ ~ 15-20 cm^{-1} is necessary to describe the lowest energy state.

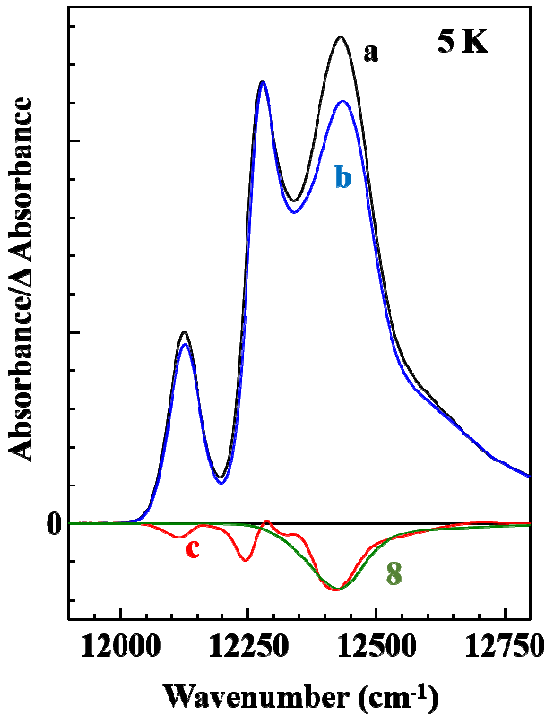

Figure 6. Absorption spectra for FMO in neutral (a) and oxidizing (b) conditions, i.e., after the addition of potassium ferricyanide. The red curve c = b – a. The green curve labeled 8 is the inverted and scaled BChl *a* 8 spectral contribution from Figure 2 with a peak position of 12,422 cm^{-1}.

Table 4. Rate constant matrix calculated for Model C (ps^{-1})

M	1	2	3	4	5	6	7	8
1	0	-1.7	-0.2	-0.1	-0.1	0	0	0
2	0	1.7	-0.7	-1.7	-0.8	-0.5	-0.2	-0.1
3	0	0	0.9	-0.6	-0.8	-0.5	-1.5	-0.2
4	0	0	0	2.4	-0.6	-0.7	-0.7	-0.4
5	0	0	0	0	2.3	-0.4	-0.7	-0.9
6	0	0	0	0	0	2.2	-0.8	-1.6
7	0	0	0	0	0	0	3.9	-0.7
8	0	0	0	0	0	0	0	4.0

In regards to the photosystem of GSB, Figure 7 shows the energy levels of FMO calculated in this work compared to the 5 K fluorescence spectrum of the chlorosome–baseplate complex of *C. tepidum*.[60] The FMO absorption covers the region from 12,100 to 12,600 cm^{-1} and exhibits spectral overlap with both the chlorosome and baseplate (BChl *a*–CsmA) fluorescence bands. The baseplate, which is spatially close to BChl *a* 1 and 6,[56] has an emission band coinciding with the spectral position of the lowest energy states of FMO. However, at room temperature this fluorescence band broadens significantly and shifts to ~12,430 cm^{-1},[21,57] which increases spectral overlap with the higher energy exciton levels. This increased spectral overlap can promote more efficient EET, as incoherent hopping is distance dependent and BChl *a* 6 and 8 have been proposed as excitation entrances to FMO due to their close proximity with the baseplate.[19,21,61] Such an arrangement is consistent with the "downhill energy funnel" model of

FMO.[57] Although the exact structure of the chlorosome–baseplate–FMO–RC (including BChl *a* distances and orientations) is not known, recent studies have reported that within 10 ps 60-70% of the exciton transfers from the chlorosome to FMO via the baseplate,[62] while FMO → RC EET is on the order of hundreds of ps.[63]

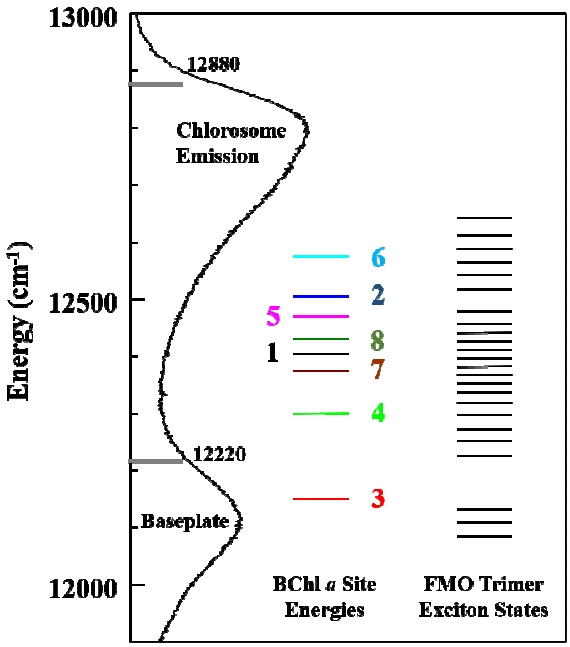

Figure 7. Energy levels of the eight BChl *a* site energies and 24 exciton states. The spectrum is the experimental fluorescence for the chlorosome–baseplate system,[60] with horizontal grey bars indicating the maxima of the zero-phonon hole action spectra for the chlorosome[64] and baseplate[60] pigments.

Conclusions

The present study (see also Supporting Information) has shown that the whole trimer, and presence of uncorrelated EET between monomers of the trimer, must be considered to explain various linear optical spectra. The Model C pigment site energies elucidated from simultaneous fits of 5 K absorption, fluorescence and persistent nonresonant HB spectra are also consistent with previously reported exciton population dynamics revealed by time-domain spectra.[43–45] BChl *a* 8 contributes to the absorption spectrum at ~12,420 cm^{-1}. This assignment contrasts the high energy values previously proposed by theoretical considerations,[21,54] but is consistent with experimental data for oxidized FMO reported in this work and ref 58. Note that *Pr. aestuarii* may have a different site energy assignment of BChl *a* 8 as evidence by the differences in, for example, absorption and CD spectra (research in progress). More detailed experimental studies (including studies of different FMO mutants) are needed to provide additional evidence about the spectral contribution of BChl *a* 8 to optical spectra.

A more accurate description of the site-dependent el-ph coupling is of interest, as dynamics and extracted site energies critically depend on the shape of the spectral density. In this work, a minimum of two spectral density shapes were necessary in order to describe the exciton population dynamics and temperature-dependent broadening. Even though molecular dynamics simulations can provide information on spectral densities,[65–67] care must be taken if using analytical forms of the energy gap correlation function; as the resulting spectral density may not describe the phonon sideband and define the *S* factor.[39] In addition, a recent study has shown the effects of force fields and quantum mechanical approaches on the spectral density shapes.[67] To date only the spectral density shape of the lowest energy state can be measured experimentally. Thus, more work is needed to extract site-dependent spectral densities from experimental data. In order to further test the Hamiltonian and el-ph coupling parameters proposed in this work, theoretical descriptions of pump-probe and 2DES frequency maps are needed to provide more insight on the population and coherence dynamics for the FMO complex, in particular on the time evolution of the 2DES rephasing and non-rephasing spectra of the FMO trimer when treated separately (research in progress).

ASSOCIATED CONTENT

Supporting Information. Summary of model parameters and spectra simulated for previously proposed Hamiltonians from the literature compared to 5 K experimental data. This material is available free of charge via the Internet at http://pubs.acs.org.

AUTHOR INFORMATION

Corresponding Author

* E-mail: ryszard@ksu.edu

Notes

The authors declare no competing financial interests.

ACKNOWLEDGMENT

This work was supported by the U.S. Department of Energy, Office of Science, Office of Basic Energy Sciences, under Award Number DE-SC-0006678 (to R.J.). Sample preparation of the FMO protein was funded by the Photosynthetic Antenna Research Center (PARC), an Energy Frontier Research Center funded by the U.S. Department of Energy, Office of Science, Office of Basic Energy Sciences, under Award Number DE-SC-0001035. The authors acknowledge useful discussion with Drs. Darius Abramavicius and Olga Rancova (Vilnius University, Lithuania) and Dr. Tonu Reinot for help in development of the software used in the present work.

REFERENCES

(1) Olson, J. M. The FMO Protein. *Photosynth. Res.* **2004**, *80*, 181–187.

(2) Milder, M. T. W.; Brüggemann, B.; van Grondelle, R.; Herek, J. L. Revisiting the Optical Properties of the FMO Protein. *Photosynth. Res.* **2010**, *104*, 257–274.

(3) Fenna, R. E.; Matthews, B. W. Chlorophyll Arrangement in a Bacteriochlorophyll Protein from Chlorobium limicola. *Nature* **1975**, *258*, 573–577.

(4) Tronrud, D. E.; Wen, J.; Gay, L.; Blankenship, R. E. The Structural Basis for the Difference in Absorbance Spectra for the FMO Antenna Protein from Various Green Sulfur Bacteria. *Photosynth. Res.* **2009**, *100*, 79–87.

(5) Larson, C. R.; Seng, C. O.; Lauman, L.; Matthies, H. J.; Wen, J.; Blankenship, R. E.; Allen, J. P. The Three-Dimensional Structure of the FMO Protein from *Pelodictyon phaeum* and Implications for Energy Transfer. *Photosynth. Res.* **2011**, *107*, 139–150.

(6) Tronrud, D. E.; Allen, J. P. Reinterpretation of the Electron Density at the Site of the Eighth Bacteriochlorophyll in the FMO Protein from *Pelodictyon phaeum*. *Photosynth. Res.* **2012**, *112*, 71–74.

(7) Ben-Shem, A.; Frolow, F.; Nelson, N. Evolution of Photosystem I – from Symmetry through Pseudosymmetry to Asymmetry. *FEBS Lett.* **2004**, *564*, 274–280.

(8) Wen, J.; Zhang, H.; Gross, M. L.; Blankenship, R. E. Native Electrospray Mass Spectrometry Reveals the Nature and Stoichiometry of Pigments in the FMO Photosynthetic Antenna Protein. *Biochemistry* **2011**, *50*, 3502–3511.

(9) MacGowan, S. A.; Senge, M. O. Contribution of Bacteriochlorophyll Conformation to the Distribution of Site-Energies in the FMO Protein. *Biochim. Biophys. Acta* **2016**, *1857*, 427–442.

(10) Anda, A.; Hansen, T.; de Vico, L. Multireference Excitation Energies for Bacteriochlorophylls A within Light Harvesting System 2. *J. Chem. Theory Comput.* **2016**, *12*, 1305–1313.

(11) Savikhin, S.; Buck, D. R.; Struve, W. S. Oscillating Anisotropies in a Bacteriochlorophyll Protein: Evidence for Quantum Beating Between Exciton Levels. *Chem. Phys.* **1997**, *223*, 303–312.

(12) Engel, G. S.; Calhoun, T. R.; Read, E. L.; Ahn, T.-K.; Mančal, T.; Cheng, Y.-C.; Blankenship, R. E.; Fleming, G. R. Evidence for Wavelike Energy Transfer Through Quantum Coherence in Photosynthetic Systems. *Nature* **2007**, *446*, 782–786.

(13) Panitchayangkoon, G.; Hayes, D.; Fransted, K. A.; Caram, J. R.; Harel, E.; Wen, J.; Blankenship, R. E.; Engel, G. S. Long-Lived Quantum Coherence in Photosynthetic Complexes at Physiological Temperature. *Proc. Natl. Acad. Sci. U.S.A.* **2010**, *107*, 12766–12770.

(14) Förster, T. Zwischenmolekulare Energiewanderung und Fluoreszenz. *Ann. Phys. (Berlin)* **1948**, *437*, 55–75.

(15) Förster, T. Delocalized Excitation and Excitation Transfer. In *Action of Light and Organic Crystals*; Sinanoğlu, O., Ed.; Modern Quantum Chemistry: Istanbul Lectures, Part III; Academic: New York, 1965; pp 93–137.

(16) Redfield, A. G. On the Theory of Relaxation Processes. *IBM J. Res. Dev.* **1957**, *1*, 19–31.

(17) Redfield, A. G. The Theory of Relaxation Processes. *Adv. Magn. Reson.* **1965**, *1*, 1–32.

(18) Renger, T.; Marcus, R. A. On the Relation of Protein Dynamics and Exciton Relaxation in Pigment-Protein Complexes: An Estimation of the Spectral Density and a Theory for the Calculation of Optical Spectra. *J. Chem. Phys.* **2002**, *116*, 9997-10019.

(19) Adolphs, J.; Renger, T. How Proteins Trigger Excitation Energy Transfer in the FMO Complex of Green Sulfur Bacteria. *Biophys. J.* **2006**, *91*, 2778-2797.

(20) Adolphs, J.; Müh, F.; Madjet, M. E.; Renger, T. Calculation of Pigment Transition Energies in the FMO Protein. *Photosynth. Res.* **2008**, *95*, 197–209, 211.

(21) Schmidt am Busch, M.; Müh, F.; Madjet, M. E.-A.; Renger, T. The Eighth Bacteriochlorophyll Completes the Excitation Energy Funnel in the FMO Protein. *J. Phys. Chem. Lett.* **2011**, *2*, 93–98.

(22) Cho, M.; Vaswani, H. M.; Brixner, T.; Stenger, J.; Fleming, G. R. Exciton Analysis in 2D Electronic Spectroscopy. *J. Phys. Chem. B* **2005**, *109*, 10542–10556.

(23) Xu, J.; Zhang, H.-D.; Xu, R.-X.; Yan, Y. J. Correlated Driving and Dissipation in Two-Dimensional Spectroscopy. *J. Chem. Phys.* **2013**, *138*, 024106.

(24) Ritschel, G.; Roden, J.; Strunz, W. T.; Eisfeld, A. An Efficient Method to Calculate Excitation Energy Transfer in Light-Harvesting Systems: Application to the Fenna-Matthews-Olson Complex. *New J. Phys.* **2011**, *13*, 113034.

(25) Ritschel, G.; Roden, J.; Strunz, W. T.; Aspuru-Guzik, A.; Eisfeld, A. Absence of Quantum Oscillations and Dependence on Site Energies in Electronic Excitation Energy Transfer in the Fenna-Matthews–Olson–Trimer. *J. Phys. Chem. Lett.* **2011**, *2*, 2912–2917.

(26) Sharp, L. Z.; Egorova, D.; Domcke, W. Efficient and Accurate Simulations of Two-Dimensional Electronic Photon-Echo Signals: Illustration for a Simple Model of the Fenna-Matthews-Olson Complex. *J. Chem. Phys.* **2010**, *132*, 014501.

(27) Ishizaki, A.; Fleming, G. R. Theoretical Examination of Quantum Coherence in a Photosynthetic System at Physiological Temperature. *Proc. Natl. Acad. Sci. U.S.A.* **2009**, *106*, 17255–17260.

(28) Chen, L.; Zheng, R.; Jing, Y.; Shi, Q. Simulation of the Two-Dimensional Electronic Spectra of the Fenna-Matthews-Olson Complex Using the Hierarchical Equations of Motion Method. *J. Chem. Phys.* **2011**, *134*, 194508.

(29) Hein, B.; Kreisbeck, C.; Kramer, T.; Rodríguez, M. Modeling of Oscillations in Two-Dimensional Echo-Spectra of the Fenna-Matthews-Olson Complex. *New J. Phys.* **2012**, *14*, 023018.

(30) Kreisbeck, C.; Kramer, T. Long-Lived Electronic Coherence in Dissipative Exciton Dynamics of Light-Harvesting Complexes. *J. Phys. Chem. Lett.* **2012**, *3*, 2828–2833.

(31) Nalbach, P.; Braun, D.; Thorwart, M. Exciton Transfer Dynamics and Quantumness of Energy Transfer in the Fenna-Matthews-Olson Complex. *Phys. Rev. E* **2011**, *84*, 041926.

(32) Liang, X.-T. Simulating Signatures of Two-Dimensional Electronic Spectra of the Fenna-Matthews-Olson Complex: By Using a Numerical Path Integral. *J. Chem. Phys.* **2014**, *141*, 044116.

(33) Kell, A.; Acharya, K.; Zazubovich, V.; Jankowiak, R. On the Controversial Nature of the 825 nm Exciton Band in the FMO Protein Complex. *J. Phys. Chem. Lett.* **2014**, *5*, 1450–1456.

(34) Herascu, N.; Kell, A.; Acharya, K.; Jankowiak, R.; Blankenship, R. E.; Zazubovich, V. Modeling of Various Optical Spectra in the Presence of Slow Excitation Energy Transfer in Dimers and Trimers with Weak Inter-Pigment Coupling: FMO as an Example. *J. Phys. Chem. B* **2014**, *118*, 2032–2040.

(35) Kell, A.; Acharya, K.; Blankenship, R. E.; Jankowiak, R. On Destabilization of the Fenna-Matthews-Olson Complex of *Chlorobaculum tepidum*. *Photosynth. Res.* **2014**, *120*, 323–329.

(36) Raszewski, G.; Renger, T. Light Harvesting in Photosystem II Core Complexes is Limited by the Transfer to the Trap: Can the Core Complex Turn into a Photoprotective Mode? *J. Am. Chem. Soc.* **2008**, *130*, 4431–4446.

(37) Renger, T.; Holzwarth, A. R. Theory of Excitation Energy Transfer and Optical Spectra of Photosynthetic Systems. In *Biophysical Techniques in Photosynthesis: Volume II*; Aartsma, T. J., Matysik, J., Eds.; Advances in Photosynthesis and Respiration, Volume 26; Govindjee, Ed.; Springer: Dordrecht, Netherlands, 2008; 99 421–443.

(38) Madjet, M. E.; Abdurahman, A.; Renger, T. Intermolecular Coulomb Couplings from Ab Initio Electrostatic Potentials: Application to Optical Transitions of Strongly Coupled Pigments in Photosynthetic Antennae and Reaction Centers. *J. Phys. Chem. B* **2006**, *110*, 17268–17281.

(39) Kell, A.; Feng, X.; Reppert, M.; Jankowiak, R. On the Shape of the Phonon Spectral Density in Photosynthetic Complexes. *J. Phys. Chem. B* **2013**, *117*, 7317–7323.

(40) Rätsep, M.; Freiberg, A. Electron-Phonon and Vibronic Couplings in the FMO Bacteriochlorophyll *a* Antenna Complex Studied by Difference Fluorescence Line Narrowing. *J. Lumin.* **2007**, *127*, 251–259.

(41) Creemers, T. M. H.; de Caro, C. A.; Visschers, R. W.; van Grondelle, R.; Völker, S. Spectral Hole Burning and Fluorescence Line Narrowing in Subunits of the Light-Harvesting Complex LH1 of Purple Bacteria. *J. Phys. Chem. B* **1999**, *103*, 9770–9776.

(42) Nelder, J. A.; Mead, R. A Simplex Method for Function Minimization. *Comput. J.* **1965**, *7*, 308–313.

(43) Freiberg, A.; Lin, S.; Timpmann, K.; Blankenship, R. E. Exciton Dynamics in FMO Bacteriochlorophyll Protein at Low Temperatures. *J. Phys. Chem. B* **1997**, *101*, 7211–7220.

(44) Savikhin, S.; Buck, D. R.; Struve, W. S. Toward Level-to-Level Energy Transfers in Photosynthesis: The Fenna–Matthews–Olson Protein. *J. Phys. Chem. B* **1998**, *102*, 5556–5565.

(45) Vulto, S. I. E.; Neerken, S.; Louwe, R. J. W.; de Baat, M. A.; Amesz, J.; Aartsma, T. J. Excited-State Strucure and Dynamics in FMO Antenna Complexes from Photosynthetic Green Sulfur Bacteria. *J. Phys. Chem. B* **1998**, *102*, 10630–10635.

(45) Reinot, T.; Chen, J.; Kell, A.; Robben, K. C.; Jassas, M.; Zazubovich, V.; Jankowiak, R. On the Conflicting Estimations of Pigment Site Energies in Photosynthetic Complexes: A Case Study of the CP47 Complex. *Anal. Chem. Insights* **2016**, *11*, 35–48.

(46) Wendling, M.; Pullerits, T.; Przyjalgowski, A.; Vulto, S. I. E.; Aartsma, T. J.; van Grondelle, R.; van Amerongen, H. Electron–Vibrational Coupling in the Fenna–Matthews–Olson Complex of *Prosthecochloris aestuarii* Determined by Temperature-Dependent

Absorption and Fluorescence Line-Narrowing Measurements. *J. Phys. Chem. B* **2000**, *104*, 5825–5831.

(47) Angell, C. A. Liquid Fragility and the Glass Transition in Water and Aqueous Solutions. *Chem. Rev.* **2002**, *102*, 2627–2649.

(48) Ringe, D.; Petsko, G. A. The 'Glass Transition' in Protein Dynamics: What It Is, Why It Occurs, and How to Exploit It. *Biophys. Chem.* **2003**, *105*, 667–680.

(49) Olson, J. M.; Ke, B.; Thompson, K. H. Exciton Interaction Among Chlorophyll Molecules in Bacteriochlorophyll *a* Proteins and Bacteriochlorophyll *a* Reaction Center Complexes from Green Bacteria. *Biochim. Biophys. Acta* **1976**, *430*, 524–537, 763.

(50) Francke, C.; Amesz, J. Isolation and Pigment Composition of the Antenna System of Four Species of Green Sulfur Bacteria. *Photosynth. Res.* **1997**, *52*, 137–146.

(51) Vulto, S. I. E.; de Baat, M. A.; Louwe, R. J. W.; Permentier, H. P.; Neef, T.; Miller, M.; van Amerongen, H.; Aartsma, T. J. Exciton Simulations of Optical Spectra of the FMO Complex from the Green Sulfur Bacterium *Chlorobium tepidum* at 6 K. *J. Phys. Chem. B* **1998**, *102*, 9577–9582.

(52) Kihara, S.; Hartzler, D. A.; Orf, G. S.; Blankenship, R. E.; Savikhin, S. *J. Phys. Chem. B* **2015**, *119*, 5765–5772.

(53) Orf, G. S.; Niedzwiedzki, D. M.; Blankenship, R. E. Intensity Dependence of the Excited State Lifetimes and Triplet Conversion Yield in the Fenna–Matthews–Olson Antenna Protein. *J. Phys. Chem. B* **2014**, *118*, 2058–2069.

(54) Olbrich, C.; Jansen, T. L.-C.; Liebers, J.; Aghtar, M.; Strümpfer, J.; Schulten, K.; Knoester, J.; Kleinekathöfer, U. From Atomistic Modeling to Excitation Transfer and Two-Dimensional Spectra of the FMO Light-Harvesting Complex. *J. Phys. Chem. B* **2011**, *115*, 8609–8621.

(55) Hayes, D.; Engel, G. S. Extracting the Excitonic Hamiltonian of the Fenna-Matthews-Olson Complex Using Three-Dimensional Third-Order Electronic Spectroscopy. *Biophys. J. 2***011**, *100*, 2043–2052.

(56) Wen, J.; Zhang, H.; Gross, M. L.; Blankenship, R. E. Membrane Orientation of the FMO Antenna Protein from *Chlorobaculum tepidum* as Determined by Mass Spectrometry-Based Footprinting. *Proc. Natl. Acad. Sci. U.S.A.* **2009**, *106*, 6134–6139.

(57) Müh, F.; Madjet, M. E.; Adolphs, J.; Abdurahman, A.; Rabenstein, B.; Ishikita, H.; Knapp, E.; Renger, T. α-Helices Direct Excitation Energy Flow in the Fenna-Matthews-Olson Protein. *Proc. Natl. Acad. Sci. U.S.A.* **2007**, *104*, 16862–16867.

(58) Bina, D.; Blankenship, R. E. Chemical Oxidation of the FMO Antenna Protein from *Chlorobaculum tepidum*. *Photosynth. Res.* **2013**, *116*, 11–19.

(59) Renge, I.; Mauring, K. Spectral Shift Mechanisms of Chlorophylls in Liquids and Solutions. *Spectrocheim. Acta A* **2013**, *102*, 301–313.

(60) Kell, A.; Chen, J.; Jassas, M.; Tang, J. K.-H.; Jankowiak, R. Alternative Excitonic Structure in the Baseplate (BChl *a*–CsmA Complex) of the Chlorosome from *Chlorobaulum tepidum*. *J. Phys. Chem. Lett.* **2015**, *6*, 2702–2707.

(61) Moix, J.; Wu, J.; Huo, P.; Coker, D.; Cao, J. Efficient Energy Transfer in Light-Harvesting Systems, III: The Influence of the Eighth Bacteriochlorophyll on the Dynamics and Efficiency in FMO. *J. Phys. Chem. Lett.* **2011**, *2*, 3045–3052.

(62) Huh, J.; Saikin, S. K.; Brookes, J. C.; Valleau, S.; Fujita, T.; Aspuru-Guzik, A. Atomistic Study of Energy Funneling in the Light-Harvesting Complex of Green Sulfur Bacteria. *J. Am. Chem. Soc.* **2014**, *136*, 2048–2057.

(63) He, G.; Niedzwiedzki, D. M.; Orf, G. S.; Zhang, H.; Blankenship, R. E. Dynamics of Energy and Electron Transfer in the FMO-Reaction Center Core Complex form the Phototrophic Green Sulfur Bacterium *Chlorobaculum tepidum*. *J. Phys. Chem. B* **2015**, *119*, 8321–8329.

(64) Pšenčík, J.; Polívka, T.; Němec, P.; Dian, J.; Kudrna, J.; Malý, P.; Hála, J. Fast Energy Transfer and Exciton Dynamics in Chlorosomes of the Green Sulfur Bacterium *Chlorobium tepidum*. *J. Phys. Chem. A* **1998**, *102*, 4392–4398.

(65) Olbrich, C.; Strümpfer, J.; Schulten, K.; Kleinekathöfer, U. Theory and Simulation of the Environmental Effects on FMO Electronic Transitions. *J. Phys. Chem. Lett.* **2011**, *2*, 1771–1776.

(66) Rivera, E.; Montemayor, D.; Masia, M.; Coker, D. F. Influence of Site-Dependent Pigment–Protein Interactions on Excitation Energy Transfer in Photosynthetic Light Harvesting. *J. Phys. Chem. B* **2013**, *117*, 5510–5521.

(67) Chandrasekaran, S.; Aghtar, M.; Valleau, S.; Aspuru-Guzik, A.; Kleinekathöfer, U. Influence of Force Fields and Quantum Chemistry Approach on Spectral Densities of BChl *a* in Solution and in FMO Proteins. *J. Phys. Chem. B* **2015**, *119*, 9995–10004.

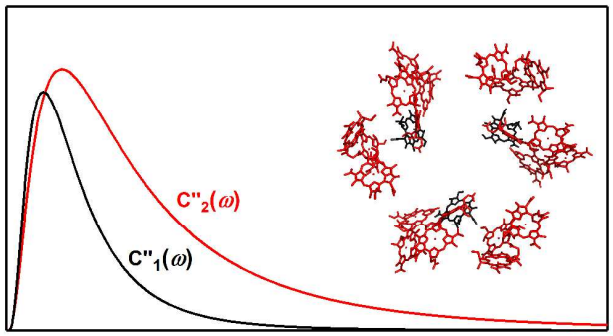

Table of Contents artwork